Single-mode guiding properties of subwavelength-diameter silica and silicon wire waveguides

Limin Tong

Division of Engineering and Applied Sciences, Harvard University, Cambridge, MA 02138, USA
ltong@fas.harvard.edu
Centre for Optical and Electromagnetic Research, State Key Laboratory of Modern Optical Instrumentation, Zhejiang University, Hangzhou 310027, China
phytong@zju.edu.cn

Jingyi Lou

Department of Physics and State Key Laboratory of Silicon Materials, Zhejiang University, Hangzhou 310027, China

Eric Mazur

Department of Physics and Division of Engineering and Applied Sciences, Harvard University, Cambridge, MA 02138, USA
Mazur@deas.harvard.edu

http://www.mazur.harvard.edu

Abstract: Single-mode optical wave guiding properties of silica and silicon subwavelength-diameter wires are studied with exact solutions of Maxwell's equations. Single mode conditions, modal fields, power distribution, group velocities and waveguide dispersions are studied. It shows that air-clad subwavelength-diameter wires have interesting properties such as tight-confinement ability, enhanced evanescent fields and large waveguide dispersions that are very promising for developing future microphotonic devices with subwavelength-width structures.

OCIS codes: (000.4430) Numerical approximation and analysis; (060.2430) Fiber, single mode; (230.7370) Waveguides; (350.3950) Micro-optics; (999.9999) Nanowire.

References and links

1. P. P. Bishnu, *Fundamentals of Fibre Optics in Telecommunication and Sensor Systems* (John Wiley & Sons, New York, NY 1993).
2. R. G. Hunsperger, *Photonic Devices and Systems* (Marcel Dekker, New York, NY 1994).
3. J. S. Sanghera, and I. D. Aggarwal, *Infrared Fiber Optics* (CRC Press, New York, NY 1998).
4. X. F. Duan, Y. Huang, R. Agarwal, and C. M. Lieber, "Single-nanowire electrically driven lasers, " Nature **421**, 241-245 (2003).
5. L. M. Tong, R. R. Gattass, J. B. Ashcom, S. L. He, J. Y. Lou, M. Y. Shen, I. Maxwell, and E. Mazur, "Subwavelength-diameter silica wires for low-loss optical wave guiding," Nature **426**, 816-819 (2003).
6. A. M. Morales, and C. M. Lieber, "A laser ablation method for the synthesis of crystalline semiconductor nanowires," Science **279**, 208-211 (1998).
7. Z. W. Pan, Z. R. Dai, C. Ma, and Z. L. Wang, "Molten gallium as a catalyst for the large-scale growth of highly aligned silica nanowires," J. Am. Chem. Soc. **124**, 1817-1822 (2002).
8. A. W. Snyder, and J. D. Love, *Optical waveguide theory* (Chapman and Hall, New York, NY 1983).
9. P. Klocek, *Handbook of infrared optical materials* (Marcel Dekker, New York, NY 1991).
10. E. D. Palik, *Handbook of optical constants of solids* (Academic Press, New York, NY 1998).
11. A. P. Abel, M. G. Weller, G. L. Duveneck, M. Ehrat, and H. M. Widmer, "Fiber-optic evanescent wave biosensor for the detection of oligonucleotides," Anal. Chem. **68**, 2905-2912 (1996).
12. M. J. Levene, J. Korlach, S. W. Turner, M. Foquet, H. G. Craighead, and W. W. Webb, "Zero-mode waveguides for single-molecule analysis at high concentrations, " Science **299**, 682-686 (2003).

#3825 - $15.00 US Received 13 February 2004; revised 8 March 2004; accepted 9 March 2004

13. C. Manolatou, S. G. Johnson, S. Fan, P. R. Villeneuve, H. A. Haus, and J. D. Joannopoulos, "High-density integrated optics, " J. Lightwave Technol. **17**, 1682-1692 (1999).
14. G. Kakarantzas, T. E. Dimmick, T. A. Birks, R. Le Roux, and P. S. Rusell, "Miniature all-fiber devices based on CO_2 laser microstructuring of tapered fibers, " Opt. Lett. **26**, 1137-1139 (2001).
15. Z. M. Qi, N. Matsuda, K. Itoh, M. Murabayashi, and C. R. Lavers, "A design for improving the sensitivity of a Mach-Zehnder interferometer to chemical and biological measurands, " Sensors Actuat. **B81**, 254-258 (2002).
16. B. E. A. Saleh and M. C. Teich, *Fundamentals of Photonics* (John Wiley & Sons, New York, NY 1991).
17. A. Ghatak, and K. Thyagarajan, *Introduction to Fiber Optics* (Cambridge University Press, Cambridge, 1998).
18. T. A. Birks, W. J. Wadsworth, and P. S. Russell, "Supercontinuum generation in tapered fibers, " Opt. Lett. **25**, 1415-1417 (2000).
19. L. F. Mollenauer, "Nonlinear optics in fibers," Science **302**, 996-997 (2003).
20. D. Marcuse, "Mode conversion caused by surface imperfections of a dielectric slab waveguide, " Bell Syst. Tech. J. **48**, 3187-3215 (1969).
21. D. Marcuse, and R. M. Derosier, "Mode conversion caused by diameter changes of a round dielectric waveguide, " Bell Syst. Tech. J. **48**, 3217-3232 (1969).
22. F. Ladouceur, "Roughness, inhomogeneity, and integrated optics, " J. Lightwave Technol. **15**, 1020-1025 (1997).
23. K. K. Lee, D. R. Lim, H. C. Luan, A. Agarwal, J. Foresi, and L. C. Kimerling, "Effect of size and roughness on light transmission in a Si/SiO_2 waveguide: experiments and model, " Appl. Phys. Lett. **77**, 1617-1619 (2000). Erratum: Appl. Phys. Lett. **77**, 2258 (2000).

1. Introduction

In the past 30 years, dielectric optical waveguides with widths or diameters from micrometers to millimeters have got successful applications in many fields such as optical communication, optical sensing and optical power delivery systems [1-3]. Photonic device applications benefit from minimizing the width of the waveguides, but fabricating low-loss optical waveguides with subwavelength diameters remains challenging because of high precision requirement. Recently, several types of dielectric submicrometer- and nanometer- diameter wires of optical qualities have been obtained [4-5]. These wires, with diameters smaller than a micrometer, are tens to thousands times thinner than the commonly used micrometer-diameter waveguides. They can be used as air-clad wire-waveguides with subwavelength-diameter cores, and building blocks in the future micro- and nano- photonic devices. However, in contrast to the well-studied optical waveguide with diameter larger than the wavelength, guiding property of subwavelength-diameter wire-waveguides has not been adequately studied. In this paper, based on exact solutions of Maxwell's equations and numerical calculations, we study basic guiding properties of subwavelength-diameter wires. We choose fused silica (SiO_2) and single crystal silicon (Si) as typical dielectric materials for our simulation under the following considerations: (1) fused silica and single crystal silicon are among the most important photonic and optoelectronic materials within the visible and near-infrared ranges; (2) both silica and silicon wires with submicrometer- or nanometer- diameters have been successfully fabricated [5-7]; (3) their optical and physical properties are well studied, and they have typical values of moderate and high refractive indices (about 1.45 for silica and 3.5 for silicon).

2. Basic model

For basic consideration, we assume that the wire has a circular cross-section, an infinite air clad, and a step-index profile. The wire diameter (D) is not very small (e.g. D>10 nm) so that the statistic parameters — permittivity (ε) and permeability (μ) — can be used to describe the responses of a dielectric medium to an incident electromagnetic field. The length of the wire is large enough (e.g. long than 10 μm) to establish the spatial steady state. We also assume that the wire is very uniform in diameter and smooth in sidewall, which has been shown achievable recently [5].

#3825 - $15.00 US Received 13 February 2004; revised 8 March 2004; accepted 9 March 2004

The mathematic model of an air-clad dielectric wire is shown in Fig. 1. Assuming the refractive indices of the wire material and the air are n_1 and n_2 respectively, then the wire has the following index profile

$$n(r) = \begin{cases} n_1, & 0 < r < a, \\ n_2, & a \le r < \infty \end{cases} \tag{1}$$

where a is the radius of the wire.

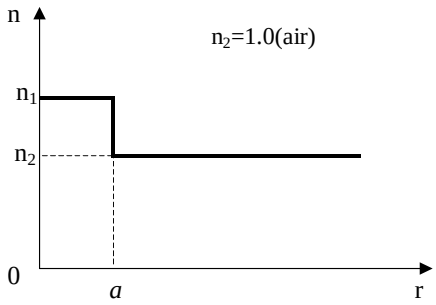

Fig. 1. Mathematic model of an air-clad cylindrical wire waveguide.

For microphotonic applications, usually a short length (e.g., tens to hundreds of micrometers) of the wire is long enough. Therefore we assume that the wire is non-dissipative and source free, which is true for most of the dielectric materials within their transparent ranges. With these assumptions, one can reduce Maxwell's equations to the following Helmholtz equations

$$\begin{aligned} \left(\nabla^2 + n^2 k^2 - \beta^2\right)\ \vec{e} = 0, \\ \left(\nabla^2 + n^2 k^2 - \beta^2\right)\ \vec{h} = 0 \end{aligned} \tag{2}$$

where $k=2\pi/\lambda$, and β is the propagation constant.

Exact solutions for this model can be found in Ref. [8]. The eigenvalue equations of Eq. (2) for various modes are as follows
for HE_{vm} and EH_{vm} modes :

$$\left\{\frac{J_v'(U)}{UJ_v(U)} + \frac{K_v'(W)}{WK_v(W)}\right\}\left\{\frac{J_v'(U)}{UJ_v(U)} + \frac{n_2^2 K_v'(W)}{n_1^2 WK_v(W)}\right\} = \left(\frac{v\beta}{kn_1}\right)^2\left(\frac{V}{UW}\right)^4 \tag{3}$$

for TE_{0m} modes :

$$\frac{J_1(U)}{UJ_0(U)} + \frac{K_1(W)}{WK_0(W)} = 0 \tag{4}$$

for TM_{0m} modes:

$$\frac{n_1^2 J_1(U)}{UJ_0(U)} + \frac{n_2^2 K_1(W)}{WK_0(W)} = 0 \tag{5}$$

where J_v is the Bessel function of the first kind, and K_v is the modified Bessel function of the second kind, $U=D(k_0^2 n_1^2-\beta^2)^{1/2}/2$, $W=D(\beta^2-k_0^2 n_2^2)^{1/2}/2$, $V= k_0 \cdot a\,(n_1^2-n_2^2)^{1/2}$, and $D=2a$.

We assume that the index of the air (n_2) is 1.0, and use the following Sellmeier-type dispersion formula (at room temperature) to obtain the refractive indices of the wire materials

#3825 - $15.00 US Received 13 February 2004; revised 8 March 2004; accepted 9 March 2004

for fused silica (SiO_2) [9]:

$$n^2 - 1 = \frac{0.6961663\lambda^2}{\lambda^2 - (0.0684043)^2} + \frac{0.4079426\lambda^2}{\lambda^2 - (0.1162414)^2} + \frac{0.8974794\lambda^2}{\lambda^2 - (9.896161)^2} \tag{6}$$

for single crystal silicon [10]:

$$n^2 = 11.6858 + \frac{0.939816}{\lambda^2} + \frac{0.000993358}{\lambda^2 - 1.22567} \tag{7}$$

where the unit of λ is μm.

Propagation constants (β) of these air-clad wire waveguides are obtained numerically. For example, shown in Fig.2 and 3 are diameter-dependent β of silica and silicon wires at the wavelength of 633 nm and 1.5 μm respectively, where the wire diameter (*D)* is directly related to the *V*-number [$V = k_0 \cdot D\ (n_1^2 - n_2^2)^{1/2}/2$]). It is clear that, when the wire diameter reduced to a certain value (denoted as D_{SM}, corresponding to V=2.405), only the HE_{11} mode exists, corresponding to the single mode operation. Several high-order modes are also plotted as dotted lines.

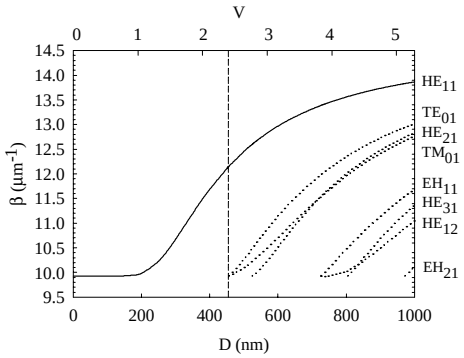

Fig. 2. Numerical solutions of propagation constant (β) of air-clad silica wire at 633-nm wavelength. Solid line, fundamental mode. Dotted lines, high-order modes. Dashed line, critical diameter for single-mode operation (D_{SM}).

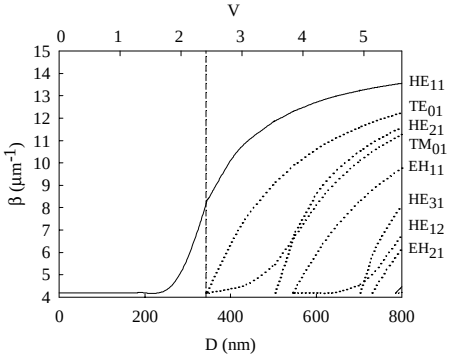

Fig. 3. Numerical solutions of propagation constant (β) of air-clad silicon wire at 1.5-μm wavelength. Solid line, fundamental mode. Dotted lines, high-order modes. Dashed line, critical diameter for single-mode operation (D_{SM}).

3. Single-mode condition and fundamental modes

The single mode condition of an air-clad wire-waveguide, as illustratively shown in Figs. 2-4 (where the dashed lines are dividing lines), can be obtained from Eqs. (4) and (5) as

$$V = 2\pi \cdot \frac{a}{\lambda_0} \cdot \left(n_1^{\,2} - n_2^{\,2}\right)^{\frac{1}{2}} \approx 2.405. \tag{8}$$

Single mode conditions of the air-clad silica- and silicon-wire waveguides with respect to the wavelengths and wire diameters, are shown as solid lines in Fig. 4. The region beneath the solid line corresponds to the single-mode region. For comparison, wavelength of the propagating light inside the wire material (that is $\lambda = \lambda_0 / n_1$) is also plotted as dashed line. It shows that, a subwavelength-diameter silica wire is always single mode, while a subwavelength-diameter silicon wire is single mode only when its diamter lays below the solid line. For example, at the wavelength of 633 nm (He-Ne laser), a silica wire with a diameter less than 457 nm will always be a single-mode waveguide; and at the wavelength of 1.5 μm, to be a single-mode waveguide, diameters of silica- and silicon-wires should be less than about 1.1 μm and 345 nm respectively. Taking into consideration that UV absorption

#3825 - $15.00 US Received 13 February 2004; revised 8 March 2004; accepted 9 March 2004

edges are about 200 nm for silica [9] and 1200 nm for silicon [10], the minimum critical diameters (D_{SM}) for silica and silicon wires are about 129 nm and 272 nm at these edges respectively. Since the interest of this work is single-mode properties, we consider the fundamental mode in the following discussion.

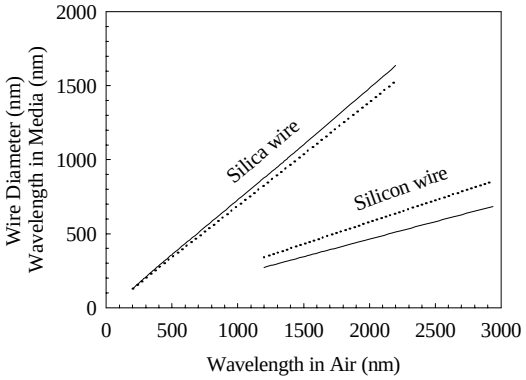

Fig. 4. Single mode condition of an air-clad silica and silicon wires. Solid line, critical diameter for single-mode operation. Dotted line, wavelength in media.

For fundamental modes (HE_{11} modes), Eq. (3) becomes

$$\left\{\frac{J_1'(U)}{UJ_1(U)}+\frac{K_1'(W)}{WK_1(W)}\right\}\left\{\frac{J_1'(U)}{UJ_1(U)}+\frac{n_2^{\,2}K_1'(W)}{n_1^{\,2}WK_1(W)}\right\}=\left(\frac{\beta}{kn_1}\right)^2\left(\frac{V}{UW}\right)^4 \tag{9}$$

with numerical solutions of the propagation constant β of the HE_{11} modes for silica and silicon at some typical wavelengths shown in Fig. 2 and Fig. 3 (solid lines). When expressing the electromagnetic fields as

$$\begin{cases}\vec{E}(r,\phi,z)=(e_r\hat{r}+e_\phi\hat{\phi}+e_z\hat{z})e^{i\beta z}e^{-i\omega t},\\ \vec{H}(r,\phi,z)=(h_r\hat{r}+h_\phi\hat{\phi}+h_z\hat{z})e^{i\beta z}e^{-i\omega t}\end{cases} \tag{10}$$

electric fields of the fundamental modes are expressed as [8]

inside the core ($0<r<a$):

$$e_r=-\frac{a_1J_0(UR)+a_2J_2(UR)}{J_1(U)}\cdot f_1(\phi), \tag{11}$$

$$e_\phi=-\frac{a_1J_0(UR)-a_2J_2(UR)}{J_1(U)}\cdot g_1(\phi), \tag{12}$$

$$e_z=\frac{-iU}{a\beta}\frac{J_1(UR)}{J_1(U)}\cdot f_1(\phi) \tag{13}$$

and outside the core ($a\le r<\infty$):

$$e_r=-\frac{U}{W}\frac{a_1K_0(WR)-a_2K_2(WR)}{K_1(W)}\cdot f_1(\phi), \tag{14}$$

#3825 - $15.00 US Received 13 February 2004; revised 8 March 2004; accepted 9 March 2004

$$e_\phi = -\frac{U}{W}\frac{a_1 K_0(WR) + a_2 K_2(WR)}{K_1(W)} \cdot g_1(\phi), \tag{15}$$

$$e_z = \frac{-iU}{a\beta}\frac{K_1(WR)}{K_1(W)} \cdot f_1(\phi) \tag{16}$$

where $f_1(\phi) = \sin(\phi), g_1(\phi) = \cos(\phi)$,

$$a_1 = \frac{F_2 - 1}{2};\ a_3 = \frac{F_1 - 1}{2},\ a_5 = \frac{F_1 - 1 + 2\Delta}{2},\ a_2 = \frac{F_2 + 1}{2},\ a_4 = \frac{F_1 + 1}{2},\ a_6 = \frac{F_1 + 1 - 2\Delta}{2},$$

$$F_1 = \left(\frac{UW}{V}\right)^2 [b_1 + (1 - 2\Delta)b_2],\quad F_2 = \left(\frac{V}{UW}\right)^2 \frac{1}{b_1 + b_2},$$

$$b_1 = \frac{1}{2U}\left\{\frac{J_0(U)}{J_1(U)} - \frac{J_2(U)}{J_1(U)}\right\},\ b_2 = -\frac{1}{2W}\left\{\frac{K_0(W)}{K_1(W)} + \frac{K_2(W)}{K_1(W)}\right\}.$$

The *h*-components can be obtained from *e*-components with some calculations and are not presented here.

Normalized electric components of the fundamental modes in cylindrical coordination for silica wires at 633-nm wavelength are shown in Fig. 5. For reference, Gaussian profiles (dashed line) are provided in the radial distributions, and the electric field of a wire with a critical diameter (D_{SM}) is also provided as a dotted line. Comparing with the Gaussian profile, air-clad silica wire shows much tighter field confinement within a certain diameter range (e.g., around 400 nm) due to the high index contrast between the air and silica. When the diameter reduces to a certain degree (e.g., 200 nm), the field begins to extend to a far distance with considerable amplitude, indicating that the majority of the field is no longer tightly confined inside or around the wire. Similar behaviors are obtained for silica and silicon wires at other wavelengths.

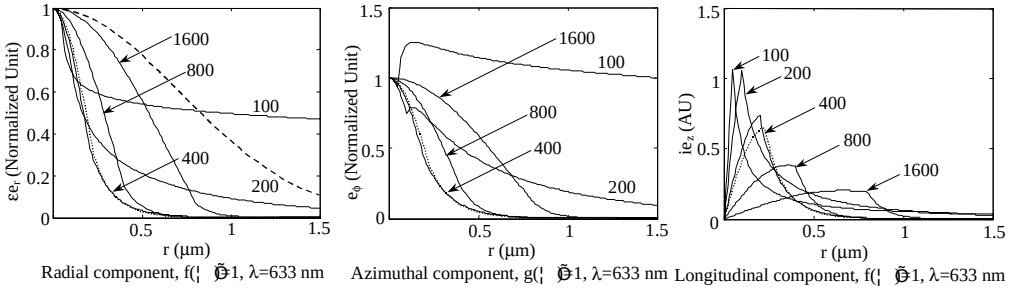

Fig. 5. Electric components of HE_{11} modes of silica wires at 633-nm wavelength with different diameters in cylindrical coordination. Normalizations are applied as: $\varepsilon e_r(r=0)=1$ and $e_\phi(r=0)=1$. Wire diameters are arrowed to each curve in unit of nm.

4. Fraction of power inside the core and effective diameter

In practical applications such as evanescent wave based optical sensing [11, 12], it is important to know the profile of the power distribution around the waveguide. For the wires considered here, the average energy flows in the radial (r) and azimuthal (ϕ) directions are zero, so we only consider the energy flow in z-direction. The z-components of Poynting vectors are obtained as [8]
inside the core ($0<r<a$):

#3825 - $15.00 US Received 13 February 2004; revised 8 March 2004; accepted 9 March 2004

$$S_{z1} = \frac{1}{2}\left(\frac{\varepsilon_0}{\mu_0}\right)^{\frac{1}{2}} \frac{kn_1^{\,2}}{\beta J_1^{\,2}(U)}\left[a_1 a_3 J_0^{\,2}(UR) + a_2 a_4 J_2^{\,2}(UR) + \frac{1-F_1F_2}{2} J_0(UR)J_2(UR)\cos(2\phi)\right] \quad (17)$$

outside the core ($a \le r < \infty$):

$$S_{z2} = \frac{1}{2}\left(\frac{\varepsilon_0}{\mu_0}\right)^{\frac{1}{2}} \frac{kn_1^{\,2}}{\beta K_1^{\,2}(W)} \frac{U^2}{W^2}\left[a_1 a_5 K_0^{\,2}(WR) + a_2 a_6 K_2^{\,2}(WR) - \frac{1-2\Delta-F_1F_2}{2} K_0(WR)K_2(WR)\cos(2\phi)\right] \quad (18)$$

Profiles of Poynting vectors for 200- and 400-nm-diameter silica wires at 633-nm wavelength are shown in Fig. 6, in which the mesh-profile stands for propagating fields inside the wire, and the gradient profile stands for evanescent fields in air. As we can see, while a 400-nm-diameter wire confines major power inside the wire, a 200-nm-diameter wire leaves a large amount of light guided outside as evanescent waves.

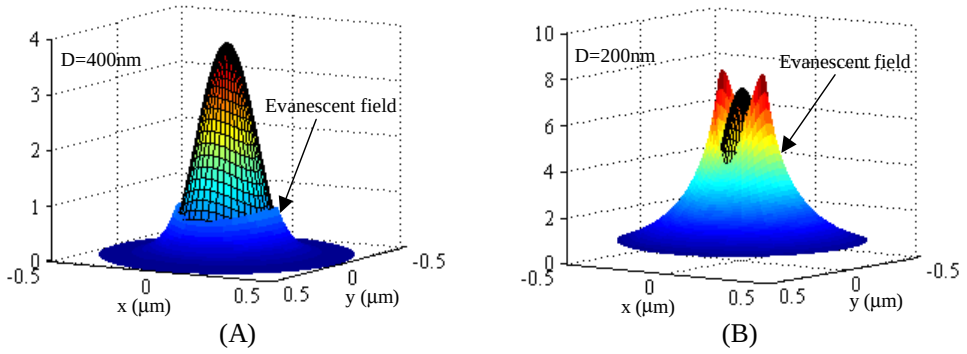

Fig. 6. Z-direction Poynting vectors of silica wires at 633-nm wavelength with diameters of (A) 400 nm and (B) 200 nm. Mesh, field inside the core. Gradient, field outside the core.

To obtain more straightforward information of the power distribution in the radial direction, we calculate the fractional power inside the core (η) and the effective diameter of the light field (D_{eff}) defined as following:

$$\eta = \frac{\int_0^a S_{z1}\,dA}{\int_0^a S_{z1}\,dA + \int_a^\infty S_{z2}\,dA} \quad (19)$$

where $dA = a^2 R \cdot dR \cdot d\phi = r \cdot dr \cdot d\phi$, and η represents the percentage of the confined light power inside the solid core. D_{eff} is obtained from

$$\begin{cases} \dfrac{\int_0^{D_{eff}} S_{z1}\,dA}{\int_0^a S_{z1}\,dA + \int_a^\infty S_{z2}\,dA} = 86.5\%, & (if\ D_{eff} \le a)\ , \\ \dfrac{\int_0^a S_{z1}\,dA + \int_a^{D_{eff}} S_{z1}\,dA}{\int_0^a S_{z1}\,dA + \int_a^\infty S_{z2}\,dA} = 86.5\%, & (if\ D_{eff} > a)\ . \end{cases} \quad (20)$$

where D_{eff} is a hypothetic diameter inside which 86.5% (that is $1\text{-}e^2$) of the total power is included.

#3825 - $15.00 US
Received 13 February 2004; revised 8 March 2004; accepted 9 March 2004

Calculated η as a function of the wire diameter (D) is shown in Fig. 7 for silica wire (633-nm and 1.5-μm wavelengths) and silicon wire (1.5-μm wavelength). It shows that, at the critical diameter (D_{SM}) (dashed line), η is about 81% for silica wire (633-nm and 1.5-μm wavelength) and 89% for silicon wire (1.5-μm wavelength). The diameter for confining 90% energy inside the core of the fundamental mode is about 566 nm (silica wire at 633-nm wavelength), 1342 nm (silica wire at 1.5-μm wavelength) and 346 nm (silicon wire at 1.5-μm wavelength), while the diameter for confining 10% energy is 216 nm (silica wire at 633-nm wavelength), 513nm (silica wire at 1.5-μm wavelength) and 264 nm (silicon wire at 1.5-μm wavelength). Tight confinement is helpful for reducing the modal width and increasing the integrated density of the optical circuits with less cross-talk [8, 13], while weaker confinement will be beneficial for energy exchanging between wires within a short interaction length [14], as well as for improving the sensitivity of evanescent wave based sensors [15].

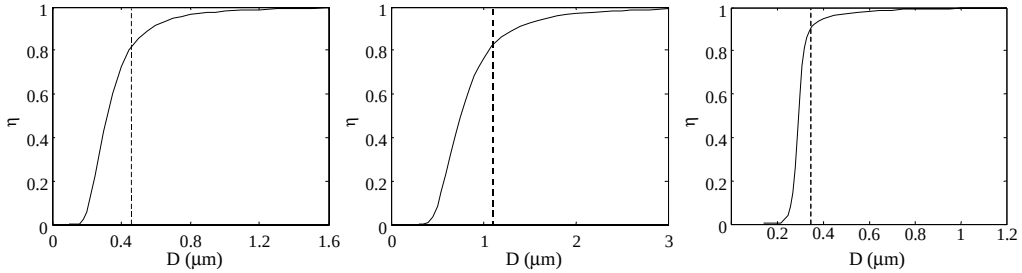

Fig. 7. Fractional power of the fundamental modes inside the core of (A) silica wire at 633-nm wavelength, (B) silica wire at 1.5-μm wavelength and (C) silicon wire at 1.5-μm wavelength. Dashed line, critical diameter for single mode operation.

The effective diameters (D_{eff}) of the fundamental modes of silica and silicon wires are shown in Fig. 8. For comparison, the real diameters of the wires are provided as dotted lines. D_{eff} is large when the wire diameter is very small, and it decreases quickly with the increasing of the wire diameter. The two curves intersect near the critical diameter (dashed line), and the real diameter exceeds the effective diameter thereafter. The intersection point represents the minimum usable wire diameter at the nominated wavelength when using an 86.5% confinement for estimation. It is clear that, a wire with a certain diameter (e.g., 450-nm-diameter silica wire at 633-nm wavelength) is able to confine the major power within a subwavelength width. In addition, D_{eff} is very larger if the wire diameter is very small. For example, at 633-nm wavelength, for silica wire with a diameter of 200 nm, D_{eff} is about 2.3 μm, which is over 10 times larger than the wire diameter. Maintaining a steady guiding field in such situation is difficult, any small deviation (such as surface contamination and micro-bends) from the ideal condition will lead to significant change in propagating fields. However, the high susceptibility of such a guiding wire may provide high sensitivity for optical sensing.

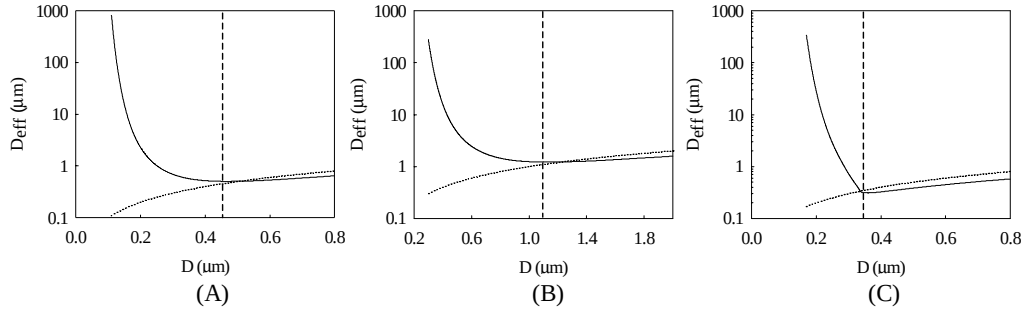

Fig. 8. Effective diameters of the light fields of the fundamental modes. Solid line, D_{eff}. Dotted line, real diameter. Dashed line, critical diameter for single mode operation. (A) silica wire at 633-nm wavelength, (B) silica wire at 1.5-μm wavelength and (C) silicon wire at 1.5-μm wavelength.

#3825 - $15.00 US Received 13 February 2004; revised 8 March 2004; accepted 9 March 2004

5. Group velocity and waveguide dispersion

Group velocity and dispersion of optical waveguides are important in many applications. Group velocity of the wire waveguide we discussed here is given as [8]

$$v_g = \frac{c}{n_1^2} \cdot \frac{\beta}{k} \cdot \frac{1}{1-2\Delta(1-\eta)}. \tag{21}$$

From which diameter-dependent group velocities of HE_{11} modes of air-clad silica and silicon wire are obtained and shown in Fig. 9. Results show that, when the wire diameter (D) is very small, v_g approaches the light speed (c) in vacuum since most of the light energy is propagated in air. When D increases, more and more energy enters the wire core, v_g decreases until it reaches a minimum value that is smaller than c/n_1. After this point, v_g increases with D. When the D is large enough, v_g finally approaching c/n_1, the group velocity of a plane wave in the wire material.

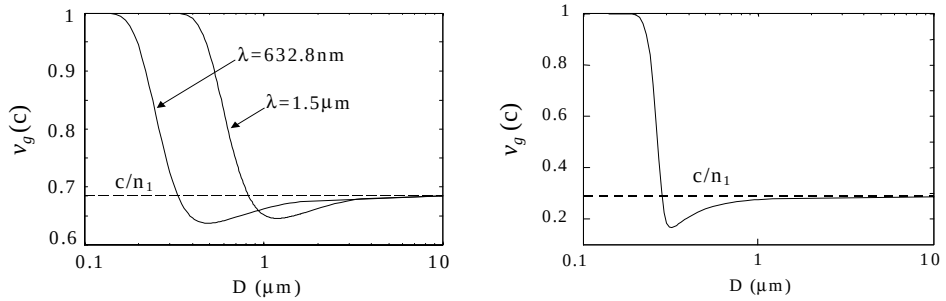

Fig. 9. Diameter-dependent group velocities of the fundamental modes of air-clad (A) silica wire at 633- nm and 1.5-μm wavelengths and (B) silicon wire at 1.5-μm wavelength.

From Eq. (21), wavelength-dependent group velocities are also obtained. As shown in Fig.10, for a given wire diameter (D), v_g approaches c when the wavelength (λ) is very larger and c/n_1 when λ is very small, with a minimum value smaller than c/n_1.

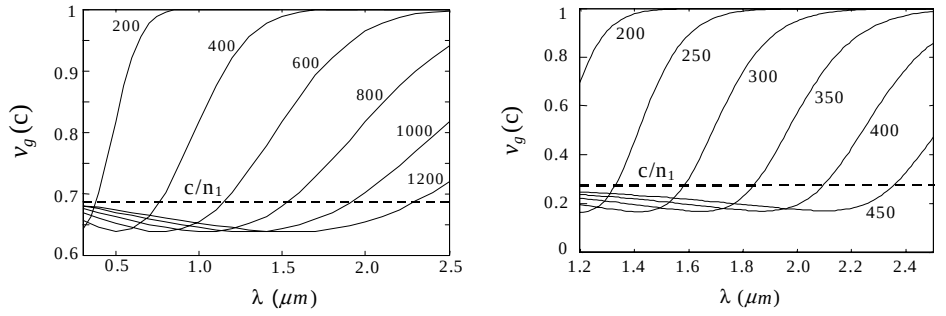

Fig. 10. Wavelength-dependent group velocities of the fundamental modes of air-clad (A) lica wire and (B) silicon wire with different diameters (wire diameters are labeled on each rve in unit of nm)

With group velocity obtained above, waveguide dispersion (D_w) is obtained as [16]

$$D_w = \frac{d(v_g^{-1})}{d\lambda}. \tag{22}$$

#3825 - $15.00 US Received 13 February 2004; revised 8 March 2004; accepted 9 March 2004

Diameter- and wavelength- dependent waveguide dispersions of air-clad silica and silicon wires are shown in Fig. 11 and Fig. 12. For reference, in Fig. 12, material dispersions of fused silica and single crystal silicon calculated from Eqs. (6) and (7) are also provided. It shows that, waveguide dispersions (D_w) of these wire-waveguides can be very large comparing with those of weakly guiding fibers and material dispersions . For example, D_w of an 800-nm-diameter silica wire at 1.5-μm wavelength is about -1400 ps/nm.km, which is about 70 times larger than that of the material dispersion. In contrast to those of ps/nm.km for weakly guided glass fibers [17], D_w of silica and silicon wires can go ns/nm.km level. Results also show that, at a particular wavelength, the total dispersion (combined material and waveguide dispersions) of a wire-waveguide can be made zero, positive or considerably negative when a proper diameter is chosen. Controlling light propagation properties by tailoring waveguide dispersion is used in many fields such as optical communication and nonlinear optics [1, 18, 19], therefore, these wires present opportunities for achieving enhanced dispersions with reduced sizes.

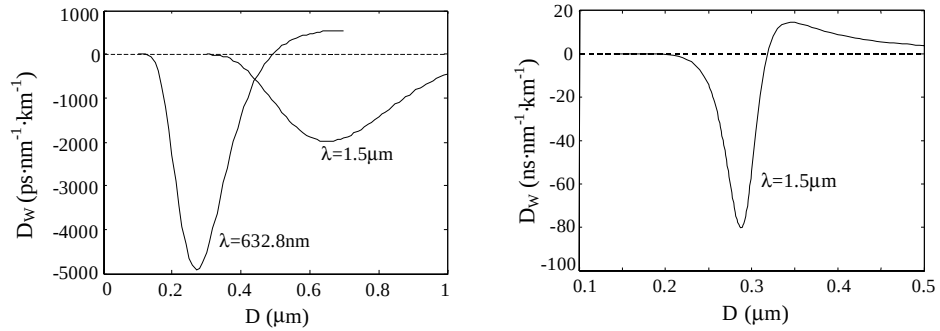

Fig. 11. Diameter-dependent waveguide dispersion of fundamental modes of air-clad (A) silica wire at 633-nm and 1.5-μm wavelengths and (B) silicon wire at 1.5-μm wavelengths.

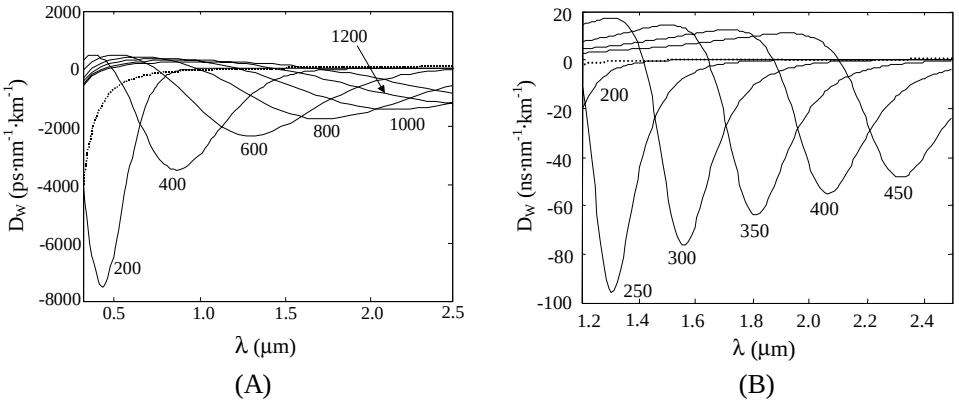

Fig. 12. Wavelength-dependent waveguide dispersion of fundamental modes of air-clad (A) silica wire and (B) silicon wire with different wire diameters (the wire diameter is labeled on each curve in unit of nm). Material dispersion is plotted in dotted line.

6. Discussions and conclusions

So far we have studied the basic properties of air-clad subwavelength-diameter silica and silicon wires for optical wave guiding. We assume that the wires are ideally uniform in terms of the sidewall smoothness and diameter uniformity. In most cases, a real wire could not be ideally uniform. However, low-loss optical wave guiding places strict requirements on the

#3825 - $15.00 US Received 13 February 2004; revised 8 March 2004; accepted 9 March 2004

sidewall smoothness and diameter uniformity [20, 21], especially when the width or diameter of the waveguide is very small [22, 23]. Therefore, practically useful wire-waveguide should have excellent uniformities to achieve low optical loss. Meanwhile, fused silica and single crystal silicon are among the most important materials for photonics, optoelectronics and electronics. Many other dielectric or semiconductor materials have refractive indices that fall between that of silica and silicon. Therefore, our results are helpful for estimating the guiding properties of many other dielectric or semiconductor wire waveguides.

Comparing with large-diameter optical waveguides, air-clad subwavelength-diameter wires show interesting properties such as enhanced evanescent fields, tight light confinement and large waveguide dispersions, which may provide opportunities for developing a number of miniaturized, high-performance and novel types of photonic devices.

Acknowledgment

This work is supported by the U.S. National Science Foundation (PHY-9988123) and the National Natural Science Foundation of China (No.60378036). The authors would like to thank Dr Sailing He, Mr R. R. Gattass and Mrs Iva Maxwell for helpful discussions. Limin Tong gratefully acknowledges support from the Center for Imaging and Mesoscale Structures at Harvard University.

#3825 - $15.00 US Received 13 February 2004; revised 8 March 2004; accepted 9 March 2004